

Non-negligible influence of vacancies and interlayer coupling on electronic properties of heavy ion irradiated $SnSe_2$ FETs

Shifan Gao(高诗凡), Siyuan Ma(马思远), Shengxia Zhang(张胜霞), Pengliang Zhu(朱彭靓), Jie Liu(刘杰), Lijun Xu(徐丽君), Pengfei Zhai(翟鹏飞), Peipei Hu(胡培培), and Yan Li(李燕)

Citation : Chin. Phys. B, 2025, 34 (**4**): 046106. DOI: 10.1088/1674-1056/adb270
Journal homepage: http://cpb.iphy.ac.cn; http://iopscience.iop.org/cpb

What follows is a list of articles you may be interested in

Investigation of heavy ion irradiation effects on a charge trapping memory capacitor by bm *C-V* measurement

Qiyu Chen(陈麒宇), Xirong Yang(杨西荣), Zongzhen Li(李宗臻), Jinshun Bi(毕津顺), Kai Xi(习凯),Zhenxing Zhang(张振兴), Pengfei Zhai(翟鹏飞), Youmei Sun(孙友梅), and Jie Liu(刘杰)
Chin. Phys. B, 2023, 32 (**9**): 096102. DOI: 10.1088/1674-1056/acae78

Effect of temperature on heavy ion-induced single event transient on 16-nm FinFET inverter chains

Li Cai(蔡莉), Ya-Qing Chi(池雅庆), Bing Ye(叶兵), Yu-Zhu Liu(刘郁竹), Ze He(贺泽), Hai-Bin Wang(王海滨), Qian Sun(孙乾), Rui-Qi Sun(孙瑞琪), Shuai Gao(高帅), Pei-Pei Hu(胡培培), Xiao-Yu Yan(闫晓宇), Zong-Zhen Li(李宗臻), and Jie Liu(刘杰)
Chin. Phys. B, 2023, 32 (**4**): 046101. DOI: 10.1088/1674-1056/ac8e9c

Lattice damage in InGaN induced by swift heavy ion irradiation

Ning Liu(刘宁), Li-Min Zhang(张利民), Xue-Ting Liu(刘雪婷), Shuo Zhang(张硕), Tie-Shan Wang(王铁山), and Hong-Xia Guo(郭红霞)
Chin. Phys. B, 2022, 31 (**10**): 106103. DOI: 10.1088/1674-1056/ac7ccd

Strategy to mitigate single event upset in 14-nm CMOS bulk FinFET technology

Dong-Qing Li(李东青), Tian-Qi Liu(刘天奇), Pei-Xiong Zhao(赵培雄), Zhen-Yu Wu(吴振宇), Tie-Shan Wang(王铁山), and Jie Liu(刘杰)
Chin. Phys. B, 2022, 31 (**5**): 056106. DOI: 10.1088/1674-1056/ac3d7e

Effect of heavy ion irradiation on the interface traps of AlGaN/GaN high electron mobility transistors

Zheng-Zhao Lin(林正兆), Ling Lü(吕玲), Xue-Feng Zheng(郑雪峰), Yan-Rong Cao(曹艳荣), Pei-Pei Hu(胡培培), Xin Fang(房鑫), and Xiao-Hua Ma(马晓华)
Chin. Phys. B, 2022, 31 (**3**): 036103. DOI: 10.1088/1674-1056/ac11e4

Non-negligible influence of vacancies and interlayer coupling on electronic properties of heavy ion irradiated $SnSe_2$ FETs

Shifan Gao(高诗凡)[1,2], Siyuan Ma(马思远)[2], Shengxia Zhang(张胜霞)[2,‡], Pengliang Zhu(朱彭靓)[2], Jie Liu(刘杰)[2], Lijun Xu(徐丽君)[2], Pengfei Zhai(翟鹏飞)[2], Peipei Hu(胡培培)[2], and Yan Li(李燕)[1,†]

[1] *Northwest Normal University (NWNU), Lanzhou* 730070, *China*
[2] *Institute of Modern Physics, Chinese Academy of Sciences (CAS), Lanzhou* 730000, *China*

(Received 2 January 2025; revised manuscript received 1 February 2025; accepted manuscript online 5 February 2025)

Influences of swift heavy ion (SHI) irradiation induced defects on electronic properties of the bulk $SnSe_2$ based FETs are explored. Latent tracks and amounts of Se vacancies in the irradiated $SnSe_2$ were confirmed. Red shift of the A_{1g} peak indicates that the resonance frequency of the phonons is reduced due to the defect generation in $SnSe_2$. The source–drain current I_{ds} increased at ion fluence of 1×10^{10} ions·cm^{-2}, which was attributeded to the irradiation caused Se vacancies, which hence increases the concentration of conduction electrons. The carrier mobility was about 16.9 cm^2·V^{-1}·s^{-1} for the devices irradiated at ion fluence of 1×10^{9} ions·cm^{-2}, which benefited from heavy ion irradiation enhanced interlayer coupling. The mechanism of device performance optimization after irradiation is discussed in detail. This work provides evidence that, given the electronic properties of two-dimensional material-based device, vacancies and interlayer coupling effects caused by SHI irradiation should not be ignored.

Keywords: heavy ion irradiation, electronic transport in nanoscale, materials structures, radiation damage, semiconductor devices

PACS: 61.80.Jh, 73.63.–b, 85.30.–z

DOI: 10.1088/1674-1056/adb270 **CSTR:** 32038.14.CPB.adb270

1. Introduction

Atomically thin sheets of two-dimensional (2D) transition metal dichalcogenides (TMDCs) have attracted interests as high-capacity electrode materials for electrochemical energy storage devices owing to their unique properties (tunable band gap, ultra-low body thickness, high surface area, and so on).[1–3] Unique physical and chemical properties of TMDCs materials allow them in a wide range applications in electronic devices, optoelectronic devices, sensors, high-performance field effect transistors (FETs) have been demonstrated in numerous TMDCs materials.[4–6] Earth-abundant and environmentally friendly tin (IV) diselenide ($SnSe_2$) is a representative member of the TMDCs. Analogous to MoS_2, $SnSe_2$ also attracted extensive attention due to its compelling application in electronics.[7] At present, there has extensive research on transistor devices of monolayer TMDCs. However, single-layer or few-layer 2D materials have significant disadvantages, such as difficulties in preparation and material instability. In contrast, $SnSe_2$ with bulk thickness have many advantages, such as higher carrier mobility; lower resistance, which can reduce energy loss; stable structure and strong process compatibility, which is convenient for large-scale production and practical applications.[8,9] Heavy ion irradiation is an excellent tool for introducing defects in the target materials. Low-energy ion implantation for regulating the performance of two-dimensional materials has been widely applied. For example, a low-energy ion sputtering method is used to modify monolayer MoS_2 in a controlled manner, which can simultaneously enhance the dipole–dipole interaction and charge transfer, thereby achieving Raman enhancement based on chemical mechanism. A team proposed a method to construct a 2D transverse p–n homojunction based on ultra-low energy ion implantation selective doping, and successfully controlled the conductive type of WS_2 by precisely adjusting the implanted ion dose.[10,11] It is generally believed that high-energy heavy ion irradiation leads to the deterioration of the devices. The dependence of ion irradiation induced defects on the electronic performance of TMDC-based FETs have been reported.[12,13] Ochedowski *et al*. reported that MoS_2 FETs deteriorate under the irradiation of a 1.14-GeV U^{28+} ion beam.[14] Zhang *et al*. have also found that the output current of $MoSe_2$ FETs decreases when irradiated by 1.8-GeV Ta ions at a fluence of 1×10^{9} ions·cm^{-2} and above.[15] In fact, some experiments have also found that the performance of the device can be optimized under a certain irradiation parameter, which is attributed to the thermal annealing effect during the irradiation process. However, the irradiation effect of heavy ions on two-dimensional materials is rather complex. As of now, other influence factors of heavy ion irradiation on the electrical per-

†Corresponding author. E-mail: liyan-nwnu@163.com
‡Corresponding author. E-mail: zhangsx@impcas.ac.cn

© 2025 Chinese Physical Society and IOP Publishing Ltd. All rights, including for text and data mining, AI training, and similar technologies, are reserved.

formance of TMDC-based devices have been rarely explored.

In this work, influences of swift heavy ion (SHI) irradiation induced defects on electronic properties of the bulk $SnSe_2$ based FETs are explored. The optimization mechanism of device performance after irradiation is discussed in detail. Se vacancies ionize adjacent Sn, promoting electron transport and increasing conductive electron concentration. Additionally, interlayer coupling effect of bulk $SnSe_2$ is enhanced after irradiation, increasing interlayer charge transfer efficiency. The research results provide a reference for the preparation of fine and controllable nanostructures in two-dimensional layered materials by SHI irradiation in the future.

2. Experimental setup

Initially, a silicon wafer with 300-nm thick layer of SiO_2 on the surface was prepared. $SnSe_2$ nanosheets were then transferred onto the SiO_2/Si wafer using mechanical exfoliation method from the bulk $SnSe_2$ crystals (Six Carbon, China). The electrode pairs on SiO_2 surface acted as the source and drain, and the heavily p-doped Si substrate served as the back gate. Metal electrodes (Ti 5 nm/Au 60 nm) were fabricated on the ends of $SnSe_2$ flakes using e-beam evaporation method. Figure 1(a) shows the schematic diagram of SHI irradiation. Figure 1(b) shows the actual device and thickness of the $SnSe_2$ sheet that was approximately 40 nm. Bulk $SnSe_2$ is tunable and stable, and bulk materials typically have higher electron conductivity.[16,17] 2.76-GeV ^{181}Ta ions with an initial kinetic energy of 16 MeV/u were provided by Heavy Ion Research Facility in Lanzhou (HIRFL) at different ion fluences ranging from 1×10^8 ions/cm^2 to 1×10^{12} ions/cm^2. The number of SHIs approaching each device was in the approximate range of 200 ions/device–1.2×10^4 ions/device. All the samples were irradiate at room temperature in a high-vacuum environment. The electronic energy loss ($e\mathrm{d}E/\mathrm{d}x$) on the surface of $SnSe_2$ was about 26.8 keV nm^{-1} and the nulcear energy loss was about 2.17×10^{-2} keV·nm^{-1}, the projected range was about 100.1 μm in $SnSe_2$ according to the stopping and range of ions in matter (SRIM) 2010 code.[18]

3. Results and discussion

Surface morphology of the irradiated $SnSe_2$ FETs was investigated by AFM, as shown in Fig. 1(c). Hillocks with height of approximately 3 nm were found in Fig. 1(c). Additionally, several protrusions with height of 5 nm were observed, which are likely residues that became attached to the surface during device transfer or storage. According to the thermal spike model, when the SHI enters the target material, it deposits energy along its path, causing excitation or ionization of the atoms along the path.[19] Energy is then transferred to the lattice atoms through electron–phonon interactions. The incident ions continuously deposit energy along its path, causing the temperature raised above the melting point of the target material. Partial melting was resulted in the irradiated target, followed by rapid cooling and eventual permanent defect damage, called latent track. Since the phonon frequency is sensitive to the crystal lattice and defects, Raman spectra of the pristine and irradiated $SnSe_2$ were characterized. Two strong peaks located at 110.2 cm^{-1} and 185.4 cm^{-1}, corresponding to the E_g (in plane) vibration mode and the A_{1g} (out of plane) vibration mode were observed in the Raman spectra of the pristine $SnSe_2$ flakes, as shown in Fig. 1(d). The mode E_g is characterized by an in-plane stretching behavior and another non-degenerate higher frequency Raman mode A_{1g} is attributed to out of plane stretching of the chalcogen atoms, as shown in Fig. 1(e).[20,21]

It is found in Fig. 1(e) that A_{1g} peak red shift for the irradiated samples. It is indicated that the resonance frequency of phonons reduced due to the generation of the defects in $SnSe_2$, which is favorable for carrier transport. We also find that the A_{1g} peak after irradiation is significantly enhanced, which is mainly due to the further influence of local stress and strong interlayer electron–phonon coupling.[22–24] More Raman spectra and variation patterns of $SnSe_2$ after ion irradiation are shown in the supplementary materials. SHI irradiation introduces stress inside the bulk $SnSe_2$, which may prompt local adjustments in the crystal structure and enhance the Raman scattering efficiency, thus making the Raman peak stronger. Additionally, the displacement of the out-of-plane Raman mode (A_{1g}) may be caused by the strong electron–phonon coupling at the material interface. Currently, defects act as a bridge to promote interlayer electron transfer, strengthening the originally weak interlayer coupling. Therefore, the defects introduced by SHI may change the charge distribution between the layers of $SnSe_2$, enhance the interlayer coupling and charge transfer efficiency, and increase the intensity of the Raman peak.

Figures 2(a)–2(c) show the TEM images of $SnSe_2$ films irradiated at different angles of incidence. The latent tracks under low ion fluence are not convenient for observation. Therefore, the ion fluence of our transmission samples is relatively high. The lattice spacing has been calculated to be 0.33 nm as shown in Fig. 2(a), which is consistent with previous literature.[25] Fourier transform plots of the red boxes were inserted in Figs. 2(a) and 2(b). Fourier transformed diffraction pattern of the selected irradiated region shows obvious amorphous halo rings. And the lattice fringes are incomplete, which indicates the chaotic and disordered atomic arrangement. Cylindrical latent tracks with an apparent length of about 38 nm were observed in Fig. 2(c). To gain a better understanding of SHI irradiation caused stoichiometric modification, we performed chemical composition analysis us-

ing energy-dispersive x-ray spectroscopy (EDX). The pristine sample, as confirmed by EDX in Fig. 2(d), has an Sn:Se ratio of approximately 1.85, which is close to the expected 1:2 stoichiometric composition of $SnSe_2$.[26] Figure 2(e) shows that the ratio of Se to Sn around the latent traces is significantly reduced to about 1:3 after irradiation with ion fluences of 3.06×10^{11} ions·cm^{-2} at an inclination angle of 15°. It is evident that Se atoms escaped from $SnSe_2$ after irradiation.

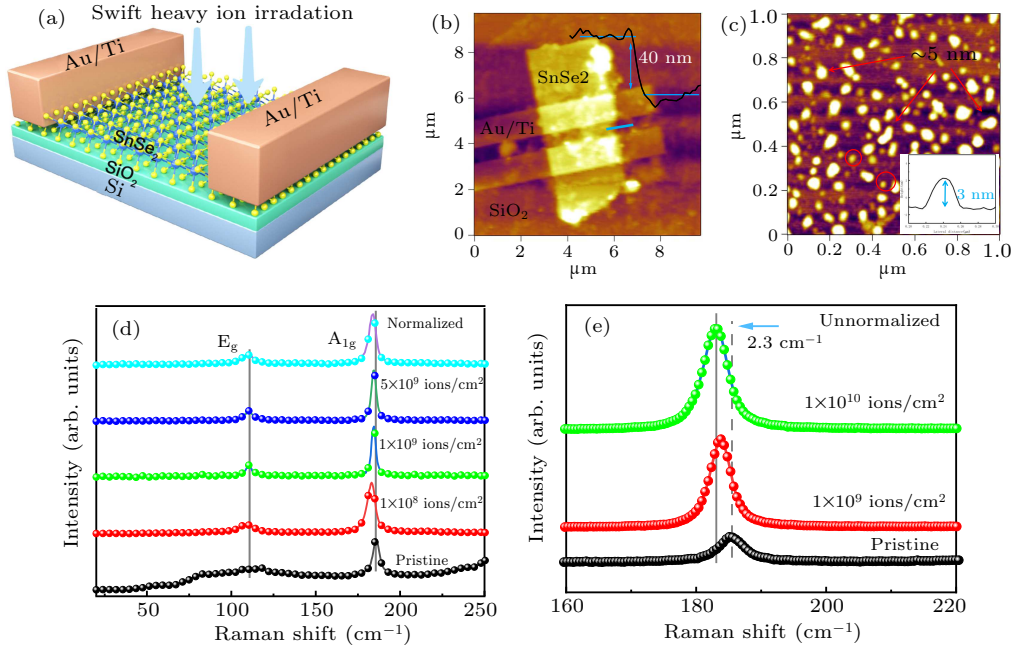


Fig. 1. (a) Schematic illustration of SHI irradiation on $SnSe_2$ FET device. (b) AFM image of one of the $SnSe_2$ FETs, and the insert shows the thickness of $SnSe_2$ flakes. (c) Surface morphology of the irradiated $SnSe_2$ flakes. (d) Raman spectrum of $SnSe_2$ under different fluences. (e) Evolution of A_{1g} peak with increasing ion fluences.

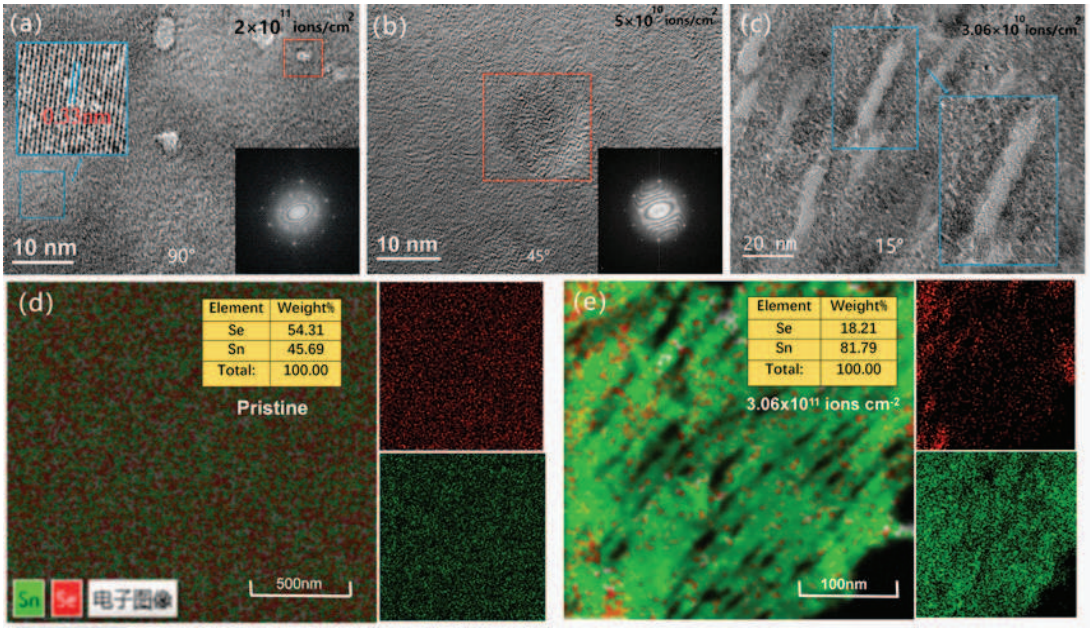


Fig. 2. (a) TEM image of the perpendicularly irradiated $SnSe_2$ with fluences of 2×10^{11} ions·cm^{-2}. (b) TEM image of the irradiated $SnSe_2$ with incident angle of 45°. The fluences was 5×10^{10} ions·cm^{-2}. (c) TEM image of irradiated $SnSe_2$ with incident angle of 15°. The fluence was 3.06×10^{11} ions·cm^{-2}. (d) and (e) EDX spectra of the pristine and irradiated $SnSe_2$.

Figure 3 shows the electrical characteristics of the pristine and SHI irradiated $SnSe_2$ FETs. Plots in Figs. 3(a) and 3(b) are the output characteristics (i.e., the source–drain current I_{ds} versus the source–drain voltage V_{ds}) measured at gate voltages (V_g) of 0.05 V and 10 V. A good linear relationship between the current and bias voltage indicates a good Ohmic contact between Ti/Au electrodes and the $SnSe_2$ sheet. The I–V output curve is measured in a voltage range of −40 mV to 40 mV to avoid Joule heating caused by excessive current at $SnSe_2$ and the metal interface. It was found that the current I_{ds} slightly

decreased when the devices were irradiated at relatively lower ion fluence 1×10^{9} ions·cm^{-2}. For example, the source current of the pristine device was about 1.6×10^{-4} A at $V_{ds} = 0.04$ V and $V_g = 0.05V$. The current I_{ds} for the irradiated devices reduced to 9.3×10^{-6} A. The value of the resistance R increased from 2.5 kΩ to 4.3 kΩ. Although the current I_{ds} dropped by two orders of magnitude, the output current I_{ds} still various with V_g for the irradiated devices, as shown in Fig. 3(a). When irradiated with ion fluence of 1×10^{10} ions·cm^{-2}, the current increased slightly, and the resistance R decreased from 3.6 kΩ to 2.2 kΩ, as shown in Fig. 3(b). The control ability of gate voltage on output current was not obvious. This could be attributed to the Fermi pinning effects. The illustration in Fig. 3(b) shows an enlarged output curve, we can observe that the control of gate voltage is relatively weak. But the device can still operate normally. When the pinning effect at the Fermi level is significant, it affects the sensitivity of the Schottky barrier height (SBH) to the metal work function, resulting in low carrier injection efficiency.[27–29] Figures 3(c) and 3(d) present the transfer curve of the pristine and irradiated $SnSe_2$ FETs. Firstly, it can be seen from the figure that the specified condition of $V_{ds} = 0.05$ V, the currents I_{ds} of the two FETs gradually increase with the increase of the voltage V_g. This indicates that the $SnSe_2$ FETs fabricated in this work are n-type FETs. Therefore, the channel material $SnSe_2$ with a bulk thickness is an n-type semiconductor. Moreover, we have preliminarily calculated that the carrier mobility of the pristine $SnSe_2$ FETs are 8.2 cm^2·V^{-1}·s^{-1} respectively. The carrier mobility of $SnSe_2$ FETs was evaluated using the following equation $\mu = [L/WC_iV_{ds}] \times [dI_{ds}/dV_g]$ where L and W are channel length and width, respectively, and C_i is the capacitance per unit area of back gate insulator, where $C_i = 11.5$ nF·cm^{-2} in this study. The bulk $SnSe_2$-based device exhibits an n-type conduction behavior with an electron mobility about 16.9 cm^2·V^{-1}·s^{-1} when irradiated with ion fluence of 1×10^{9} ions·cm^{-2}. The mobility of few-layer $SnSe_2$ prepared by mechanical exfoliation method was reported to be 8.6 cm^2·V^{-1}·s^{-1} at room temperature.[30] While the carrier mobility was about 4 cm^2·V^{-1}·s^{-1} for the devices irradiated at ion fluence of 1×10^{10} ions·cm^{-2}.

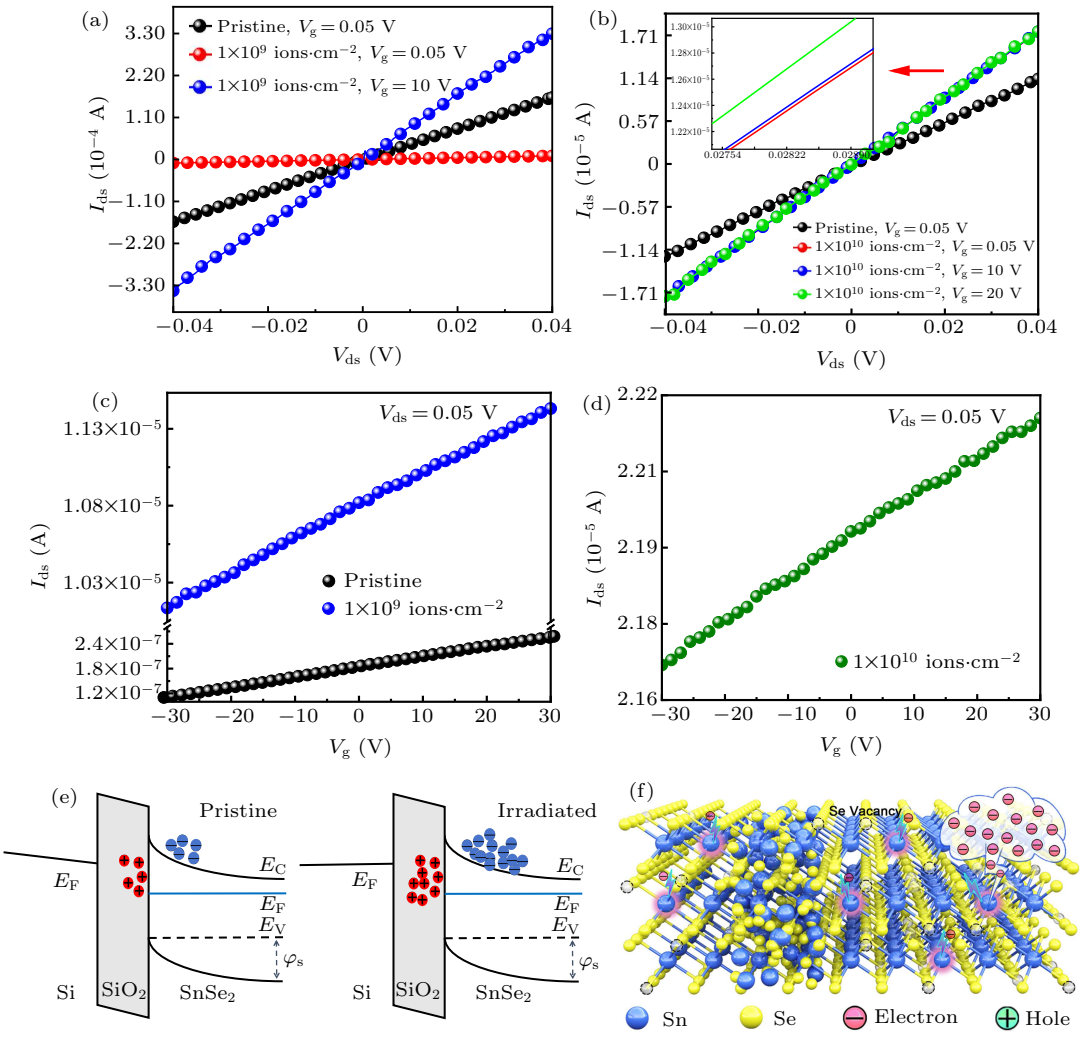


Fig. 3. (a) The output curve before and after 1×10^{9}-ions·cm^{-2} irradiation. (b) The output curve before and after 1×10^{10}-ions·cm^{-2} irradiation. (c)–(d) The transfer curves after irradiation of 1×10^{9} ions·cm^{-2} and 1×10^{10} ions·cm^{-2}, respectively. (e) Band diagrams after irradiation. (f) Schematic diagram of Sn ionization around Se vacancies in the defective bulk $SnSe_2$.

Generally, the optimized and degraded properties of the devices could be ascribed to the competition among defect scattering, localization, and local annealing effect. Defects can form Anderson localized states in semiconductors.[31] Defect concentration leads to the conductivity transition from semiconductor state to weakly localized state and further disorder leads to strongly localized state.[32] Besides, defects can also act as scattering center and affect the carrier transport directly. Transportation mechanisms of carriers in amorphous latent tracks were discussed in detail by Zhang.[33] Therefore, the defect localization and scattering lead to the decreased output current of the device irradiated by 1×10^9 ions·cm^{-2}. The formation energy of Se vacancy is about 1.75 eV.[34] Interestingly, it was found that Se vacancies in $SnSe_2$ thin films could provide opportunity for adjacent Sn ionization, resulting in concentrated conductive electrons, as schematically shown in Fig. 3(f). Accompanied with the generation of Se vacancies, the surrounding Sn atoms were attracted to the positive charge of the vacancies, which further changes the energy level of these Sn atoms.[35] Hence, electrons in the valence band are more likely to jump to the conduction band, which increases the concentration of conduction electrons, as shown in Fig. 3(e). Li *et al*. also found that the loss of Se atoms in SnSe leads to a narrowing of the band gap of SnSe, and a certain amount of vacancy can also increase the mobility of electrons.[36] In addition, the red shift of A_{1g} peak for the irradiated $SnSe_2$ indicates that the phonon scattering is weakened, which is beneficial to the electron transport. Hence, the optimized electrical performance of $SnSe_2$ FETs was attributed to three simultaneous effects: (i) The loss of Se atoms leads to a narrowing of the $SnSe_2$ band gap and a change in the Fermi level, and the Se vacancies cause the ionization of adjoining Sn. These two aspects promote electron transport and increase the concentration of conduction electrons. (ii) A certain level of vacancies can reduce the scattering between electrons and lattice vibrations, increasing the mobility of electrons. Except for latent track caused carrier localization, vacancies can reduce phonon scattering to some extent, increase conduction electron concentration, and finally optimize the performance of electronic devices. (iii) Irradiation enhanced interlayer coupling of bulk $SnSe_2$ FETs, resulting in an enhanced interlayer charge transfer efficiency. And it is also improved the gate-control ability of the devices.

4. Conclusion

To summarize, influences of SHI irradiation induced defects on electronic properties of the bulk $SnSe_2$ based FETs are explored. Latent tracks and distortion of the crystal lattice of the irradiated $SnSe_2$ were observed. The existence of a large number of Se vacancies was confirmed. Red shift of the A_{1g} peak indicates that the resonance frequency of the phonons is reduced due to the defect generation in $SnSe_2$. Current I_{ds} increased when the devices were irradiated at a fluence of 1×10^{10} ions·cm^{-2}. This is attributed to Se vacancies in the channel material, which hence increases the concentration of conductive electrons. The carrier mobility was about 16.9 cm^{2}V^{-1}s^{-1} for the devices irradiated at ion fluence of 1×10^9 ions·cm^{-2}, which is due to SHI irradiation enhanced interlayer coupling. This work provides evidence that vacancies and interlayer coupling caused by SHI irradiation should not be ignored.

Acknowledgements

Project supported by the National Natural Science Foundation of China (Grant Nos. 12375261, 12175287, 12205350, and 62234013) and the Youth Innovation Promotion Association of the Chinese Academy of Sciences (Grant No. 2022424). We would like to thank all the accelerator staff of HIRFL of Institute of Modern Physics, Chinese Academy of Sciences.

References

[1] Soares D M, Mukherjee S and Singh G 2020 *Chemistry - A European Journal* **26** 6320
[2] Voiry D, Yang J and Chhowalla M 2016 *Adv. Mater.* **28** 6197
[3] Chhowalla M, Liu Z and Zhang H 2015 *Chem. Soc. Rev.* **44** 2584
[4] Wang Q H, Kourosh K Z , Kis A, Coleman J N and Strano M S 2012 *Nat. Nanotechnol.* **7** 699
[5] Song H S, Li S L, Gao L, Xu Y, Ueno K, Tang J, Cheng Y B and Tsukagoshi K 2013 *Nanoscale* **5** 9666
[6] Larentis S, Fallahazad B and Tutuc E 2012 *Appl. Phys. Lett.* **101** 223104
[7] Ding Y, Xiao B, Tang G and Hong J 2017 *J. Phys. Chem. C* **121** 225
[8] Deng T, Gao Z, Qiu P, Wei T, Xiao J, Wang G, Chen L and Shi X 2022 *Adv. Sci.* **9** 2203436
[9] Sledzinska M, Dimoulas A, Sotomayor Torres Clivia M and Sachat El A 2021 *Nano Lett.* **21** 9172
[10] Pan X, Zhou X, Liao X, Yu R, Yu K, Lin S, Ding Y, Luo W, Yan M and Mai L 2022 *ACS Mater. Lett.* **4** 2622
[11] Kang Y, Pei Y, He D, Xu H, Ma M, Yan J, Jiang C, Li W and Xiao X 2024 *Light: Science & Applications* **13** 127
[12] Kang Y, Pei Y, He D, et al De D, Manongdo J, See S, Zhang V, Guloy A and Peng H 2012 *Nanotechnology.* **24** 25202
[13] Lin Z, Carvalho B R, Kahn E, Lv R, Rao R, Terrones H, Pimenta M A and Terrones M 2016 *2D Mater.* **3** 022002
[14] Ochedowski O, Marinov K, Wilbs G, Keller G, Scheuschner N, Severin D, Bender M, Maultzsch J, Tegude F J and Schleberger M 2013 *J. Appl. Phys.* **113** 214306
[15] Zhang S X, Liu J, Zeng J, Hu P P, Maaz K, Xu L J, Duan J L, Zhai P F, Li Z Z and Liu L 2019 *J. Phys. D: Appl. Phys.* **52** 125102
[16] Ding Y, Xiao B, Tang G and Hong J 2017 *J. Phys. Chem. C* **121** 225
[17] Deng T, Gao Z, Qiu P, Wei T, Xiao J, Wang G, Chen L and Shi X 2022 *Adv. Sci.* **9** 2203436
[18] Ziegler J F, Ziegler M D and Biersack J P 2010 *Nucl. Meth. Phys. Res. B* **268** 1818
[19] Levalois M and Marie P 1999 *Nucl. Meth. Phys. Res. B* **64** 156
[20] Li H, Zhang Q, Yap C C R, Tay B K, Edwin T H T, Olivier A and Baillargeat D 2012 *Adv. Funct. Mater.* **22** 1385
[21] Smith A J, Meek P E and Liang W Y 1977 *J. Phys. C: Solid State Phys.* **10** 1321
[22] Wang Y and Chhowalla M 2021 *Nat. Rev. Phys.* **4** 101
[23] Zheng Y H, Zhao H, Li W, Chen Z, Zhu W, Liu X, Tang Q, Wang H, Wang C and Li Z 2023 *Appl. Phys. Lett.* **123** 251602
[24] Lu H, Zang H, Lai Z, An W, Ni V, Rodionova V, Magomedov K and Ren X 2024 *Appl. Phys. Lett.* **124** 232105

[25] Li X, Li L, Zhao H, Ruan S, Zhang W, Yan P, Sun Z, Liang H and Tao K 2019 *Nanomaterials* **9** 1324
[26] Zhang Y, Shi Y, Wu M, Zhang K, Man B and Liu M 2018 *Nanomaterials* **8** 515
[27] Wang Y Y, Huang P, Ye M, Quhe R, Pan Y Y, Xiao L, Pan F and Lu J 2017 *Chem. Mater.* **29** 2191
[28] Wang Y Y, Ye M, Weng M, Li J, Zhang X, Zhang H, Guo Y, Pan Y Y, Xiao L, Liu J, Pan F and Lu J 2017 *ACS Appl. Mater. Interfaces.* **9** 29273
[29] Liu X F, Xing K, Tang C S, Sun S, Chen P, Qi D C, Breese M B H, Fuhrer M S, Wee A T S and Yin X 2024 *Prog. Mater. Sci.* **117** 101390
[30] Su Y, Ebrish M A, Olson E J and Koester S J 2013 *Appl. Phys. Lett.* **103** 263104
[31] Anderson P W 1958 *Phys. Rev.* **109** 1492
[32] Zion E, Haran A, Butenko A V, Wolfson L, Kaganovskii Yu, Havdala T, Sharoni A, Naveh D, Richter V, Kaveh M, Kogan E and Shlimak I 2015 *Graphene.* **4** 45
[33] Zhang S X, Liu J, Zeng J, Hu P P, Maaz K, Xu L J, Duan J L, Zhai P F, Li Z Z and Liu L 2019 *J. Phys. D: Appl. Phys.* **52** 125102
[34] Zhou X Y, Liu C, Song L T, Zhang H M, Huang Z W, He C L, Li B L, Lin X H, Zhang Z C, Shi S, Shen D Y, Song R, Li J, Liu X Q, Zou X M, Huang L, Liao L, Duan X D and Li B 2022 *Science China Physics, Mechanics & Astronomy* **65** 276811
[35] Sharma J, Singh R, Singh H, Singh T, Singh P, Thakur A and Tripathi S K 2017 *J. Alloys Compd.* **724** 62
[36] Li F, Chen H, Xu L, Zhang F, Yin P, Yang T, Shen T, Qi J, Zhang Y, Li D, Ge Y and Zhang H 2021 *ACS Appl. Mater. Interfaces.* **13** 33226